

ACTIVE PERCOLATION ANALYSIS OF PYRAMIDAL NEURONS OF SOMATOSENSORY CORTEX: A COMPARISON OF WILD TYPE AND p21H-Ras^{Val12} TRANSGENIC MICE

LUCIANO DA FONTOURA COSTA and MARCONI SOARES BARBOSA*

*Instituto de Física de São Carlos, Universidade de São Paulo
Caixa Postal 369, CEP 13560.970, São Carlos, SP, Brazil*

**marconi@if.sc.usp.br*

ANDREAS SCHIERWAGEN

*Institute for Computer Science
University of Leipzig, D-04109 Leipzig, Germany*

ALÁN ALPÁR, ULRICH GÄRTNER and THOMAS ARENDT

*Department of Neuroanatomy
Paul Flechsig Institut for Brain Research
University of Leipzig, D-04109 Leipzig, Germany*

Received 2 November 2004

Revised 27 November 2004

This article describes the investigation of morphological variations among two sets of neuronal cells, namely a control group of wild type rat cells and a group of cells of a transgenic line. Special attention is given to singular points in the neuronal structure, namely the branching points and extremities of the dendritic processes. The characterization of the spatial distribution of such points is obtained by using a recently reported morphological technique based on forced percolation and window-size compensation, which is particularly suited to the analysis of scattered points, presenting several coexisting densities. Different dispersions were identified in our statistical analysis, suggesting that the transgenic line of neurons is characterized by a more pronounced morphological variation. A classification scheme based on a canonical discriminant function was also considered in order to identify the morphological differences.

Keywords: Neuronal shape; neuromorphometry; percolation; phase transition; density analysis.

1. Introduction

During brain development, neurons form complex dendritic and axonal arbors that reach a characteristic pattern and size.¹ The development of arbor shape is partly determined by genetic factors and partly by interactions with the surrounding tissue.^{2–4} Dendritic growth is known to be responsive to various environmental

signals, including synaptic activity and guidance molecules.^{3,5,6} The impact of neurotrophins upon cortical neurons has gained special interest, since they are essential for neuronal development, as well as for the maintenance of functional stability and plasticity in the adult nervous system.^{7–10}

Both neuronal activity and neurotrophins guide dendritic development via GTPase-dependent mechanisms.^{5,11,12} Recent studies have drawn attention onto the small G-protein p21Ras in dendritic growth.^{13–15} Like other GTPases, p21Ras regulates the phosphorylation of downstream kinases, which trigger cascade mechanisms, resulting in the regulation of enzymatic activities, ionic channels, cellular morphology and gene expression.^{16–18}

Effects of p21Ras have been shown to be essential for the normal functioning and plasticity of both the developing^{19–21} and the adult nervous systems.^{22–24} Furthermore, enhanced expression of p21Ras is associated with neuronal restructuring after lesion or in the context of neurodegenerative diseases.^{25–27}

The effect of constitutively active p21Ras protein upon the mature nervous system has been previously investigated in p21H-Ras^{Val12} transgenic mice.^{13,14,28} In this model, the expression of transgenic p21H-Ras^{Val12} starts postnatally around day 15, when neurons are postmitotic and the majority of synaptic contacts has been established. In particular cortical pyramidal neurons express the transgenic construct at high levels. The volume of the cerebral cortex of these transgenic mice is increased by approximately 20% compared to wild type mice. This increase has been attributed to the enlarged volume of the cortical pyramidal cells, but not to a raise in the number of neurons.^{13,14,28,29}

Dendritic morphology of pyramidal cells is very heterogeneous, not only in different areas³⁰ but also within the same region.³¹ To set the population of neurons for investigation, only commissural neurons of layers II/III of the primary somatosensory cortex have been analyzed in this study. By means of this restriction, the analysis of a relatively homogeneous subpopulation of pyramidal neurons became possible.

In a previous study, we found that enhanced p21Ras activity results in a dramatically enlarged dendritic tree. In both cortical layers II/III and V, the total surface area and the total volume of dendritic trees is greatly increased. This is mainly caused by the increased dendritic diameter and by the appearance of additional segments.³²

On the other hand, topological complexity of pyramidal neurons in layers II/III appeared hardly affected: Sholl analysis of both basal and apical dendrites revealed no differences between transgenic and wild type mice regarding any parameters considered, i.e., numbers of intersections, branching points and tips.³²

These results suggest a rather proportional increase of dendritic tree size, without distinct changes in the space-filling properties. The aim of the present study was to substantiate these findings.

In the present work, we consider the use of a new procedure, known as percolation transform,^{33,34} which is particularly useful for characterization of spatial

density of distributed points. This framework represents an enhanced alternative to the multiscale fractal analysis reported before.³⁵ The percolation transform procedure consists of two steps. The first is to induce an active percolation dynamics by performing an exact dilation of the points. During this process, the number of mergings between points and connected groups of points is recorded for each dilation radius. Having recorded the accumulative number of mergings as a function of scale, an essential normalization procedure is performed in order to compensate for sparser distributions which would have produced a much weaker signal otherwise.

The overall enhanced sensitivity is a direct consequence of recording only mergings or shocks between the growing clusters, an abrupt phenomena which may occur at any dilation radius, rather than the smooth increase in area as considered in the (multiscale) fractal analysis.³⁵ This enhanced type of analysis is particularly suitable in the present case because the percolation transform approach is independent of size-related parameters like area and volume of the neuronal cells. We argue that changes in the global character of the percolation transform curves, derived from the reference points (i.e., dendrite extremities and branch points) of the dendrites of pyramidal neurons due to transgenic activation of p21Ras in the primary somatosensory cortex of mice, correlate with changes in the complexity of neuronal morphology.

2. Materials and Methods

2.1. *Biological*

We used data derived from experiments with three transgenic mice aged nine months (see Refs. 28 and 29 for the establishment of the transgenic mouse line), as well as with three wild type mice of the same age. All experimental procedures on animals were carried out in accordance with the European Council Directive of 24 November 1986 (86/609/EEC) and had been approved by the local authorities. All efforts were made to minimize the number of animals used and their suffering.

Mice were anaesthetised with Hypnomidate[®] (Janssen-Cilag) (1 ml/40 g body weight intraperitoneally) and positioned in a stereotaxic apparatus. Prior to incision 0.1 ml Xylonest[®] (Astra) was injected below the skin, the left parietal bone was partially removed. Using a Hamilton syringe for unilateral injection, Biotinylated Dextran Amine (1 l 20% BDA, 10.000 nominal molecular weight (MW), Molecular Probes) was mechanically delivered into the corpus callosum 1 mm lateral to the midline and 0.5 mm caudal to the bregma, 1 mm deep from pial surface according to the stereotaxic atlas of Frankin and Paxinos (1997). Seven days after surgery, the animals were intracardially perfused in deep anaesthesia, first with saline (0.9% NaCl) for 1–2 min and then with a fixative containing 4% paraformaldehyde in 0.1 M phosphate buffer (pH 7.4) for 30 min. The brains were postfixed in the same solution overnight, immersed in 30% sucrose for another 24 h, and sectioned (160 μm) in the coronal plane on a cryostat. The free-floating sections were extensively washed in 0.05 M Tris Buffered Saline (TBS, pH 7.4), and then reacted with

the avidin-biotin-peroxidase complex (1:100 in TBS, VECTASTAIN[®] Elite ABC kit, Vector Laboratories, Inc.) at room temperature for 2 h. BDA was visualized by using 3, 3-diamino-benzidine (Sigma, 0.025%) intensified with nickel-ammonium sulphate (Merck, 0.05%) in the presence of 0.001% hydrogen peroxide, diluted in TBS. Sections were mounted onto gelatine coated glass slides, dehydrated and covered with DPX (Fluka, Neu-Ulm, Germany).

The retrogradely labeled pyramidal cells were reconstructed using NeuroLucida[®] (MicroBrightField, Inc.), see Fig. 1. The system allowed accurate tracing of the cell processes in all three dimensions and continuous adjustment of the dendritic diameter with a circular cursor. A motorized stage with position encoders enabled the navigation through the section in the *xyz* axes and the accurate acquisition of the spatial coordinates of the measured structure. All visible dendrites were traced without marking eventual truncation of smaller dendritic sections. This may have led to certain underestimation of the dendritic tree, especially in transgenic

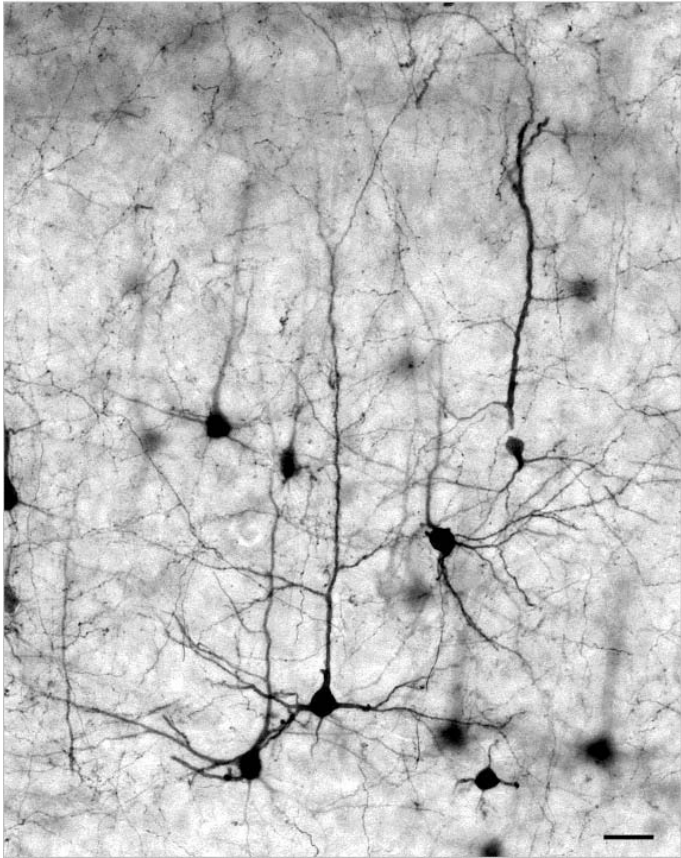


Fig. 1. Retrogradely pyramidal neurons in layers II/III of the primary somatosensory cortex. Scale bar: 50 μ m.

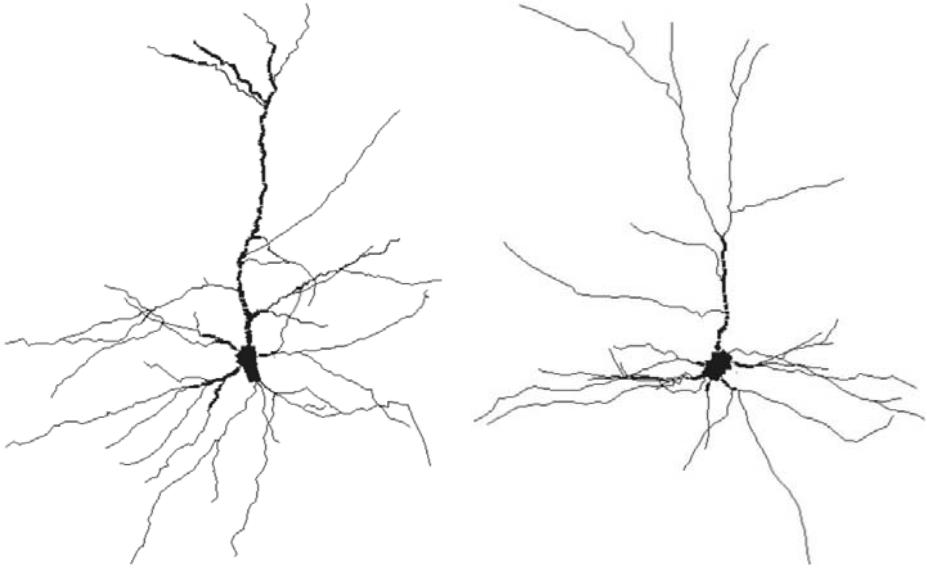


Fig. 2. Pyramidal cells rendered with Cvapp. Displayed are random examples of each transgenic neuron (cell SE8, left) and wild type neuron (cell WT19, right).

mice with a larger dendritic arbour. To gain both optimal transparency for optimal tracing facilities and at the same time a possibly complete neuronal reconstruction, sections of $160\ \mu\text{m}$ thickness were used. Thicker sections allowed only ambiguous tracing of thinner dendritic branches. Shrinkage correction (300%) was carried out in the z axis, but not in the xy plane, because shrinkage was negligible in these dimensions (10%).

The morphology files created by NeuroLucida[®] need to be edited and converted to a simpler file format before they can be used for further analyses. We used for this purpose the freely available program Cvapp.³⁶ Cvapp is a cell viewing, editing and format converting program for morphology files, see Fig. 2. It can be also used to prepare structures digitized with NeuroLucida[®] software for modeling with simulators like Neuron and Genesis. There are helpful guidelines on how to use cvapp to convert NeuroLucida ASCII files to the SWC format describing the structure of a neuron in the simplest possible way.³⁷

Each line encodes the properties of a single neuronal compartment. The format of a line in a SWC file is as follows: $nTxyzRP$. In turn, these numbers mean: (1) an integer label (normally increasing by one from one line to the next) that identifies the compartment, (2) an integer that represents the type of neuronal segment (0-undefined, 1-soma, 2-axon, 3-dendrite, 4-apical dendrite, etc.), (3)–(5) xyz coordinate of compartment, (6) radius of compartment, (7) parent compartment (defined as -1 for the initial compartment). The sample of neurons edited, converted and analyzed (see below) comprised 28 of wild type neurons and 26 of transgenic neurons.

2.2. Computational

The concept of percolation transform^{33,34} is described in the following. As mentioned in Sec. 1, this method uses a mechanism known as Minkowski dilation. Given a set of points S in R^3 , its Minkowski dilation by a radius r corresponds to the union of closed balls of radius r_i placed over each point in S , and the volume of the dilated set is represented as $V(r_i)$. In order to ensure enhanced precision and computational efficiency, only those radiuses corresponding to the possible distances in the orthogonal lattice, the so-called exact distances,³⁸ are taken into account.

Consider now that the set of points S is generated from a Poisson distribution with density γ inside a cubic window of side L . Let $C(d_i)$ be a function that counts the number of mergings between growing clusters at a specific distance $d_i = 2r_i$ as the whole set of points undergoes a dilation by radius r_i . In order to allow scale uniformity, we make the change of variables $k_i = \ln(d_i)$. A graphic representation of this function is shown in Fig. 3 for two different values of density γ_1 and γ_2 . One can see that there is a characteristic scale for each density, where most of the merging dynamics takes place before reaching a plateau. The total number of points in S is given by $\gamma_1 V$ or $\gamma_2 V$ as illustrated by Fig. 3. The idealized scenario where this dynamics occurs is represented by the unit step functions. In our model, the position of such a transition is taken as the characteristic scale for the set S .

Next, we need to relate the characteristic scales to the densities of the generated Poisson set of points. We argue that the distance where all points suddenly collapse into a unique cluster is in fact the mean nearest neighbor distance. Knowing the nearest neighbor distance distribution³⁹ for the three-dimensional space, the mean nearest neighbor distance as a function of the density of the cloud can be expressed as

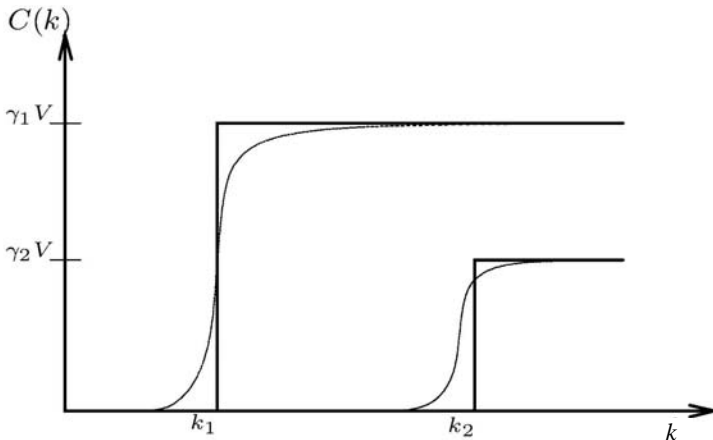


Fig. 3. The smooth curve shown corresponds (schematically) to the accumulative mergings as a function of the characteristic scale for a Poisson distribution of points. The unit-step functions shown come from idealized assumptions.

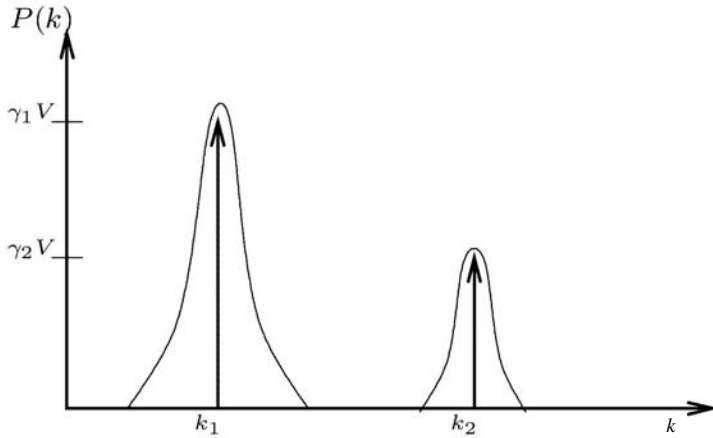


Fig. 4. The derivative of the cumulative merging function, as a function of the characteristic scale. Schematically as before, the smooth curves stands for Poisson clouds and the Kronecker functions, represented as upward arrows, are associated with the idealized model.

$$\bar{d} = \frac{0.554}{\sqrt[3]{\gamma}}. \tag{1}$$

The derivative of the cumulative number of mergings function, $C(d_i)$, is show schematically in Fig. 4. The smooth curve represents the behavior of the shock dynamics for a Poisson model, while the un-normalized Dirac deltas stand for the idealized model. Note that the rate of change of the cumulative number of mergings for higher scales tends to decrease fastly. As we intend to use these characteristic scales to detect multiple densities coexisting in the same set of points, we need a normalization procedure in order to enhance the signal for sparser distributions of points, therefore assigning the same importance to all scales. To implement such a normalization, we take as reference the maximum value of the rate of change for one specific reference scale k_j . The function we need should always give the same value irrespectively of the characteristic scale we are dealing with, as in the following equation

$$Q(\bar{k}_i) = \frac{P(\bar{k}_i)}{\Delta \bar{k}_j} e^{(3\bar{k}_i - 3\bar{k}_j)}. \tag{2}$$

This normalization procedure is the last step in the percolation approach. In the case of an experimental cumulative function obtained from a Poisson simulation with specific density, Eq. (2) will produce the same intensity for any density value. When dealing with an experimental cumulative function involving an unknow mixture of densities, Eq. (2) will yield the multiple characteristic distances actually occuring in the sampled space.

We illustrate the potential of this procedure on coexisting densities of spatially distributed points for the following experimental example. Figure 5 presents an example pattern (inset) and the corresponding percolation transform curve. The

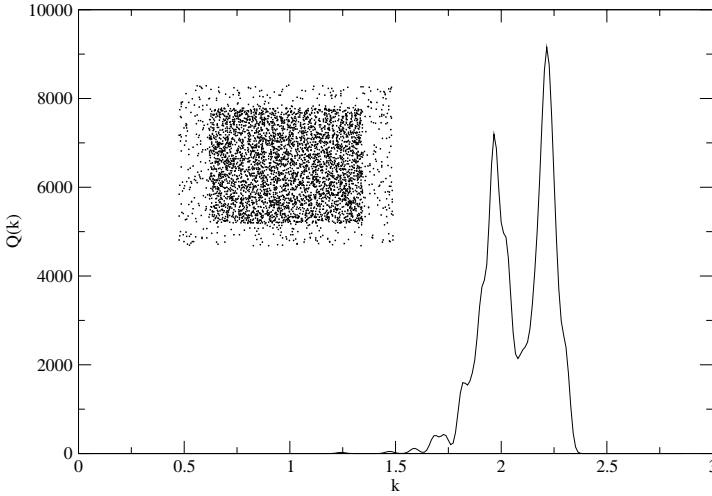


Fig. 5. An example showing the resolving ability of the proposed procedure for the pattern shown in the inset. The two coexisting densities are clearly detected by the peaks occurring at their characteristic scales.

example pattern consists of two Poisson clouds with distinct densities. The percolation curve for this example shows clearly the two peaks corresponding to the characteristics scales associated with the two different densities. Note that the difference in height of those peaks reflects the relative area occupied by each cloud.

In the present work, we consider the spatial distribution of the singular points of the dendritic trees, i.e., dendritic branch points and extremities. Such an approach^{40,41} has shown to be an effective route when dealing with subtle geometrical changes while considering a single morphological/physiological class of neuronal cells.

3. Results

Figure 6 shows the resulting percolation transform curve for the two selected cells of Fig. 2. The overall profile of these curves were the same, showing two prominent peaks at clearly distinguishable scales.^a Although we can see that these two single cells present a clearly distinct global features in their signature curve, this property is masked by the statistical variabilities of the whole set of cells, as shown by the scatter plot in Fig. 7. This scatter plot is an example of various quantile–quantile graphs we produced using global properties of all percolation curves, such as those exemplified in Fig. 6. For this purpose, we select a few global properties, namely the mean, the variance, the maximum value, the scale at which the maximum value occur and the monotonicity index.⁴² The scatter plot of Fig. 7 is defined by the monotonicity index and the maximum scale, as an example of the overall variability

^aNote that the scale axis is the natural logarithm of the actual distance among the points.

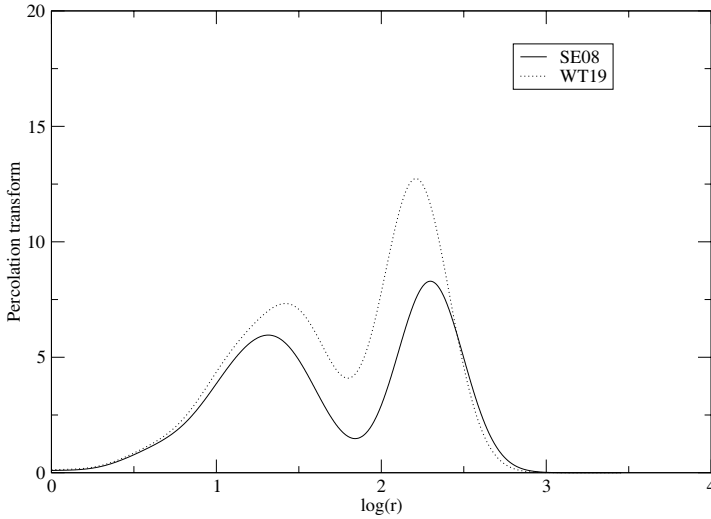


Fig. 6. Example of the percolation curve for the two types of neuronal cells presented in Fig. 2.

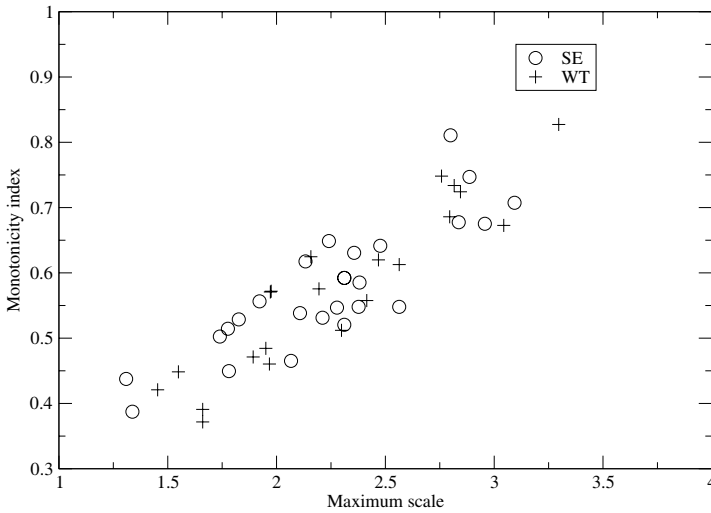


Fig. 7. A scatter plot defined by the monotonicity index (vertical axis) and the scale (horizontal axis) at which the maximum of the percolation transform curve occurs.

of shapes. Taken pairwise, none of these global measures leads to clear separation of the two types of cell involved in this study.

Before ruling out the possible existence of a geometrical characteristic that may be correlated with the genetic treatment, we performed a more thorough statistical analysis of the data produced by the percolation approach. These consist of a principal component analysis and a canonical discriminant analysis.⁴³ Figure 8

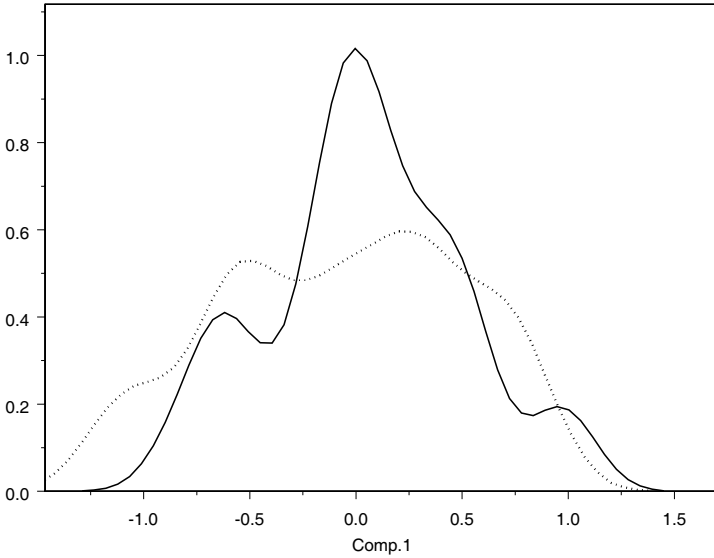


Fig. 8. The density profile of the principal component score for each class in this experiment. One can see a very similar mean and broader dispersion in the WT cells shown by the dotted line.

Table 1. The result of classical discriminant analysis for the measures considered in the scatter plot of Fig. 7. From this cross-validation table, we observe a somewhat better classification rate for type SE while for WT, the estimation is indecisive.

	SE	WT	Error	Posterior. Error
SE	20	7	0.2592593	0.3891051
WT	9	12	0.4285714	0.4767072
Overall			0.6878307	0.4274310

shows the density profile for the principal component variable, showing a similar mean but a pronounced difference in dispersion of the considered geometrical features of the genetically treated cells. Table 1 shows the performance of these selected global features in providing a discriminant function for the two type of cells. While there is visible potential for classifying one type of cells, namely the SE group, the discriminant function has a marginal performance concerning the other group, misclassifying almost half of them. This can be graphically visualized in Fig. 9.

4. Discussion

The present study is one of the few which uses 3D data on neuronal morphology to quantitatively characterize the complexity and scaling properties of different neuron types. The morphology of pyramidal cells was investigated in two sets of

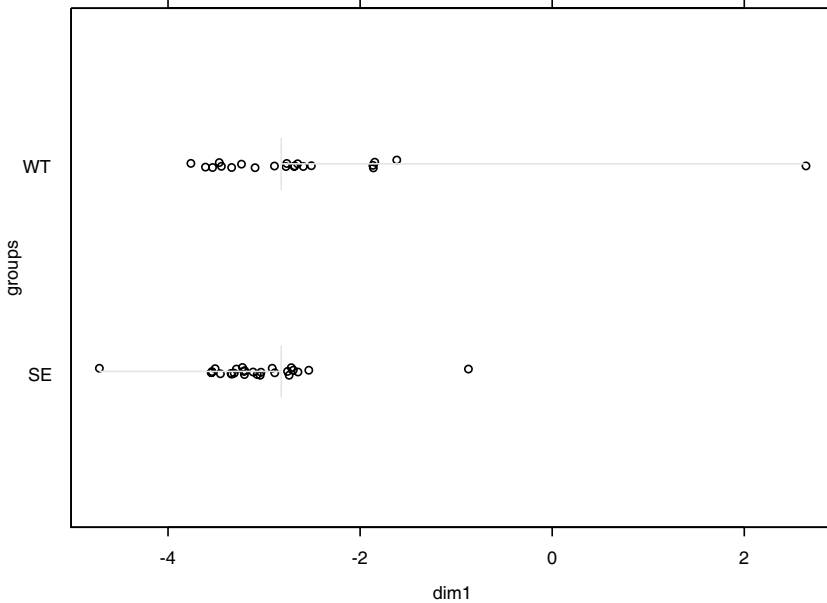


Fig. 9. The graphical result of canonical analysis, showing the amount of discrimination possible for both classes of neurons with one-dimensional variable.

neurons, i.e., wild type and p21H-Ras^{Val12} transgenic mice. The results obtained using principal component analysis indicates that the transgenic neurons have a greater dispersion, as revealed by the density profiles shown in Fig. 8. This finding may suggest that the enhanced p21Ras activity in transgenic mice may lead to greater variety of the cell morphological phenotype.

These results must be valued with care, however. We know from other studies (e.g., Fernandez *et al.* 1994) that a measure like fractal dimension for example is not sufficient to differentiate between cell classes. Alone, it does not completely specify a cell morphology but increases classification accuracy as an additional parameter for morphological classification among several other parameters typically used for placing nerve cells in different classes such as soma diameter, maximum dendritic diameter, number of branches, etc. The same situation may have occurred here with the percolation transform approach. Although our findings suggest that transgenic mice pyramidal neurons exhibit a more variable dendritic morphology than the corresponding wild type neurons, this problem must be investigated in more detail. Clearly, such study will include a more extended statistical analyses of the neuronal morphometrical parameters.

Acknowledgments

This study was partly supported by the Deutsche Forschungsgemeinschaft (grant GA716/1-1), FAPESP and CNPq.

References

1. M. L. Feldman, *Cellular Components of the Cerebral Cortex*, Vol. 1, eds. E. G. Jones and A. Peters (Plenum Press, New York, 1984), pp. 123–200.
2. F. D. Miller and D. R. Kaplan, *Curr. Opin. Neurobiol.* **13**, 391 (2003).
3. E. K. Scott and L. Luo, *Nat. Neurosci.* **4**, 359 (2001).
4. R. O. Wong and A. Ghosh, *Nat. Rev. Neurosci.* **3**, 803 (2002).
5. A. K. McAllister, *Cereb. Cortex* **10**, 963 (2000).
6. K. L. Whitford, P. Dijkhuizen, F. Polleux and A. Ghosh, *Annu. Rev. Neurosci.* **25**, 127 (2002).
7. H. Thoenen, *Science* **270**, 593 (1995).
8. A. M. Davies, *Curr. Biol.* **10**, R198 (2000).
9. E. J. Huang and L. F. Reichardt, *Annu. Rev. Neurosci.* **24**, 677 (2001).
10. A. K. Allister, *Results Probl. Cell Differ* **39**, 89 (2002).
11. Z. Li, C. D. Aizenman and H. T. Cline, *Neuron* **33**, 741 (2002).
12. W. C. Sin, K. Haas, E. S. Ruthazer and H. T. Cline, *Nature* **419**, 475 (2002).
13. M. Holzer, U. Gärtner, F. J. Klinz, F. Narz, R. Heumann and T. Arendt, *Neuroscience* **105**, 1031 (2001).
14. M. Holzer, L. Rödel, G. Seeger, U. Gärtner, F. Narz, C. Janke, R. Heumann and T. Arendt, *Neuroscience* **105**, 1041 (2001).
15. E. J. Huang and L. F. Reichardt, *Annu. Rev. Biochem.* **72**, 609 (2003).
16. N. G. Ahn, *Mol. Cell Biochem.* **127**, 201 (1993).
17. E. Nishida and Y. Gotoh, *Trends Biochem. Sci.* **18**, 128 (1993).
18. R. Heumann, *Curr. Opin. Neurobiol.* **4**, 668 (1994).
19. M. Noda, M. Ko, A. Ogura, D. G. Liu, T. Amano, T. Takano and Y. Ikawa, *Nature* **318**, 73 (1985).
20. D. Bar-Sagi and J. R. Feramisco, *Cell* **42**, 841 (1985).
21. I. Guerrero, H. Wong, A. Pellicier and D. E. Burstein, *J. Cell Physiol.* **129**, 71 (1986).
22. R. Brambilla, N. Gnesutta, L. Minichiello, G. White, A. J. Roylance, C. E. Herron, M. Ramsey, D. P. Wolfer, V. Cestari and C. Rossi-Arnaud, *Nature* **390**, 281 (1997).
23. A. J. Silva, P. W. Frankland, Z. Marowitz, E. Friedman, G. Lazlo, D. Cioffi, T. Jacks and R. Bourtschuladze, *Nat. Genet.* **15**, 281 (1997).
24. B. D. Moore, J. M. Slopis, E. F. Jackson, A. E. De Winter and N. E. Leeds, *Neurology* **54**, 914 (2000).
25. L. L. Phillips and E. T. Belardo, *Neuroscience* **58**, 503 (1994).
26. U. Gärtner, M. Holzer and T. Arendt, *Neuroreport* **6**, 1313 (1995).
27. U. Gärtner, M. Holzer and T. Arendt, *Neuroscience* **91**, 1 (1999).
28. R. Heumann, C. Goemans, D. Bartsch, K. Lingenhöhl, P. C. Waldmeier, B. Hengerer, P. R. Allegrini, K. Schellander, E. F. Wagner, T. Arendt, R. H. Kamdem, K. Obst-Pernberg, F. Narz, P. Wahle and H. Berns, *J. Cell Biol.* **151**, 1537 (2000).
29. R. Heumann, F. Narz, Y. Algür, D. Bartsch, M. Hüser, F. J. Klinz, E. Wagner, H. Berns, K. Obst-Pernberg and P. Wahle, *J. Brain Res.* **37**, 585 (1996).
30. G. N. Elson and K. S. Rockland, *Cereb. Cortex* **12**, 1071 (2002).
31. H. Duan, S. L. Wearne, J. H. Morrison and P. R. Hof, *Neuroscience* **114**, 349 (2002).
32. A. Alpár, K. Palm, A. Schierwagen, T. Arendt and U. Gärtner, Expression of constitutively active p21h-Ras^{Val12} in postmitotic pyramidal neurons results in increased dendritic size and complexity (2003), submitted.
33. L. da F. Costa, Actively-induced percolation: An effective approach to multi-object systems characterization (2004), arXiv:cond-mat/04.
34. L. da F. Costa, Biological sequence analysis through the one-dimensional percolation transform and its enhanced version, *Bioinformatics* (2004).

35. L. da F. Costa, E. T. M. Manoel, F. Faucereau, J. Chelly, J. van Pelt and G. Ramakers, *Network: Comput. Neural Syst.* **13**, 283 (2002).
36. R. C. Cannon, Structure editing and conversion with cvapp (2000), <http://www.compneuro.org/CDROM/nmorph/usage.html>.
37. D. Jaeger, Directions on how to use cvapp to convert neurolucida v3 files to genesis 2.1 .p file format, <http://www.compneuro.org/CDROM/docs/fileconversion.html>.
38. L. da F. Costa, *International Workshop on Synthetic-Natural Hybrid Coding and Three Dimensional Imaging* (Santorini, Greece, 1999), pp. 214–217.
39. S. Torquato, B. Lu and J. Rubinstein, *J. Phys. A: Math. Gen.* **23**, 103 (1990).
40. M. S. Barbosa, L. da F. Costa and E. S. Bernardes, *Phys. Rev. E.* **67**, 061910 (2003).
41. D. A. Sholl, *J. Anat.* **87**, 387 (1953).
42. M. S. Barbosa, L. da F. Costa, *et al.*, *Eur. Phys. J. B* **37**, 109 (2003).
43. G. J. McLachlan, *Discriminant Analysis and Statistical Pattern Recognition* (Wiley, 1992).